Extended Abstracts of the 2006 International Conference on Solid State Devices and Materials, Yokohama, 2006, pp. 986-987

F-7-3

P-SONOS and N-SONOS Transient Current and Field Modeling for Program and Erase

Pei-Ying Du and Jyh-Chyurn Guo
E-mail: jcguo@mail.nctu.edu.tw, Tel : 886-3-5131368, Fax : 886-3-5724361
Institute of Electronics, National Chiao-Tung University, 1001 Ta-Hsueh Rd, Hsinchu, Taiwan, R.O.C.

ABSTRACT — Transient current models with time and field dependence are developed for SONOS cell device design focusing on PGM/ERS speed optimization. The time dependence follows asymptotic t^{-1} behavior with slower tunneling rate for ERS than PGM. The field dependence follows FN tunneling in higher field for PGM and intermediate field for ERS with relatively higher corner field for saturation. The models have been justified for P- and N-SONOS with splits of ONO scheme.

I. INTRODUCTION

NVM devices in SNOS/MNOS family have been investigated for more than 30 years. Recently, SONOS becomes a hot topic and increasing publications report the study on field dependence of PGM and ERS currents [1-3]. However, relatively fewer studies to explore the transient current behavior and the time dependence of both fields and current through the composite dielectric structure. In this work, we derive time dependent fields in bottom oxide (B.O.) and top oxide (T.O.) for both P- and N-SONOS based on band structures and transient V_T behavior under PGM and ERS. Transient current models of time and field dependence are subsequently developed with simple formulas of physics-based parameters. The analytical model of physical and structural parameters can help on SONOS cell device design for PGM/ERS speed optimization.

II. SONOS CELL STRUCTURES & OPERATION SCHEMES

Both P-channel and N-channel SONOS cell devices were fabricated by 0.18μm CMOS technology with various ONO thicknesses, as shown in Table 1. The B.O. and T.O. were formed by thermal oxidation on Si substrate and nitride, respectively. Table 2 indicates cell PGM and ERS operation schemes, both using Fowler-Nordheim tunneling (FNT) mechanism for P-SONOS and N-SONOS.

III. RESULTS AND DISCUSSION

A. PGM & ERS Speed – ONO Electric Field Modeling

Figs.1 show the ERS characteristics of P-SONOS and N-SONOS cell devices in which regions I, II, and III distinguished by apparently different ERS speeds are interpreted by the band diagrams in Fig.2 where the electron tunneling from nitride traps to Si substrate contributes the primary source for ERS (regions I, II) and the secondary source from gate through T.O. to nitride acts as a competing factor leading to saturation (region III). The obviously worse saturation revealed by N-SONOS at much lower $|\Delta Vt|$ as compared to P-SONOS can be explained by the band diagram with P^+ gate replaced by N^+ gate, which will contribute much more electron injection from gate to nitride and the early saturation at lower $|\Delta Vt|$. Figs.3 show the T.O. thickness (t_{TO}) effect on PGM speed for P-SONOS and N-SONOS. We see obvious degradation of PGM speed by thicker t_{TO} of 70Å as compared to thinner t_{TO} of 62Å. As for ERS, similar results of t_{TO} effect on ERS speed are measured, as shown in Figs.1 but with apparently worse saturation revealed by N-SONOS due to the enhanced electron injection from N^+ gate suggested by Fig.2. It is recognized that trap location is one of primary factors affecting the field distribution and current transport. In this work, the proposal of trap location at nitride/T.O. interface corresponding to T.O. formation by thermal oxidation on nitride [1] is validated by a universal tunneling characteristics. Based on the validated trap location, the electric fields under PGM calculated by our model for composite ONO dielectric structure as given by (1) for B.O. and T.O. respectively are shown in Fig.4(a). The fields at B.O. (E_{BO}) decrease with increasing t_{TO} and PGM time. As for the fields at T.O. (E_{TO}), the thicker t_{TO} leads to lower E_{TO} but revealing an opposite trend w.r.t. PGM time. Note that the E_{TO} is always larger than E_{BO} during PGM.

$$E_{BO} = \frac{|V_{ONO}| \pm \Delta V_t}{t_{ONO}}, \quad E_{TO} = \frac{|V_{ONO}|}{t_{ONO}} \mp \frac{\Delta V_t \times d_{trap}}{(t_{ONO} - d_{trap}) \times t_{ONO}} \qquad (1)$$

(E_{BO}:" – " for PGM, " + " for ERS, E_{TO}:" + " for PGM, " – " for ERS)

where $|V_{ONO}|$ is potential drop across the ONO films, $\Delta V_t \equiv V_t - V_{t,i}$, $V_{t,i}$ is the initial threshold voltage with neutral traps, t_{ONO} is the effective oxide thickness of the ONO films and d_{trap} is the trap centroid location from Si substrate and B.O. interface. Regarding the electric fields under ERS, similar results of t_{TO} effect and timing trend are shown in Fig.4(b). However, E_{TO} is always smaller than E_{BO}, which is opposite to PGM case.

B. Transient Current Model – Asymptotic t^{-1} Behavior

The transient currents extracted by $J=(dV_t/dt)\times(\varepsilon_0\varepsilon_{ox}/t_{TO})$ under PGM are shown in Fig.5(a) for P- and N-SONOS. A universal curve governed by model of $J(t)=2\times10^{-7}$A-s/cm$^2\times t^{-1}$ is identified for all the transient currents under various biases ($V_{gd}=V_g-V_d$) and t_{TO} to follow in long enough time domain, i.e. an asymptotic t^{-1} behavior. Regarding the ERS condition, all the transient currents shown in Fig.5(b) follow the asymptotic t^{-1} model by $J(t)=4\times10^{-7}$A-s/cm$^2\times t^{-1}$ in time domain of around 10ms~1s. The good match with the transient current by asymptotic t^{-1} model in our study can be explained by the formulas derived by *H. Bachhofer, et al* [4] in which $J=1/(\beta\gamma)/(t+1/J_0\beta\gamma)$ can be approximated by $J\fallingdotseq(1/\beta\gamma)\times t^{-1}$ at long enough time ($t>>1/J_0\beta\gamma$), β is the tunneling probability factor, $\gamma=1/(k_1C_{ONO})$ and $k_1 \fallingdotseq 1.55$. The larger $1/\beta\gamma$ for ERS (4×10^{-7}A-s/cm^2) as compared with PGM (2×10^{-7}A-s/cm^2) suggests the smaller β for erasing the trapped electrons in nitride than that for programming the free electrons in Si substrate.

C. Transient Current Model – Field Dependence

The field dependence of injection currents during PGM is presented by J vs. E_{BO} in Figs.6. For both P- and N-SONOS, there exist two regions for every curve under different V_{gd} in which J vs. E_{BO} follows FNT in higher field region given by (2) [4] but dramatic drop in lower field region. Regarding ejection current during ERS, J vs. E_{BO} for P- and N-SONOS are shown in Figs.7 where three regions of current transport are revealed by initial high ejection, FNT in very narrow region and followed by dramatic current drop at relatively higher E_{BO} than that of PGM. The dramatic current drop is corresponding to region III in Figs.1 and 2 due to gate injection as a competing component. The FNT current given by (3) [4] due to electron ejection from nitride traps can provide a unified curve to cover every narrow FNT region under different V_{gd}. The band diagram in Fig.8 defines the barrier heights Φ_1 and Φ_t responsible for electron injection from substrate (PGM) and ejection from nitride traps (ERS), respectively.

$$J = \frac{m_0}{m_{ox}} \frac{q^3}{16\pi^2\hbar\alpha} \times E_{ox}^2 \frac{1}{q\Phi_1} \exp\left[-\frac{4\sqrt{2m_{ox}}(q\Phi_1)^{3/2}\zeta}{3q\hbar E_{ox}}\right] \qquad (2)$$

$$J = \frac{m_0}{m_N} \frac{q^3}{16\pi^2\hbar} \times E_N^2 \frac{1}{q\Phi_t} \exp\left[-\frac{4\sqrt{2m_N}(q\Phi_t)^{3/2}}{3q\hbar E_N}\right] \qquad (3)$$

Assuming field-dependent barrier heights $\Phi_1(V_{gd})$ shown in the inset of Figs.6 for P- and N-SONOS under PGM, precise fitting to individual FNT current under various V_{gd} can be achieved. $\Phi_1(V_{gd})$ just follows linear curve with Φ_1=3.01~3.18V/3.13~3.31V for P/N-SONOS, respectively. Similar results are demonstrated for ERS shown in the inset of Figs.7 with good linear $\Phi_t(V_{gd})$ but lower values in 1.75~1.845V and 1.77~1.87V for P- and N-SONOS. Figs.6 and 7 reveal important insights as follows. (i) The device with thicker t_{TO} has lower tunneling barrier. The smaller gate injection associated with thicker t_{TO} is proposed responsible for the larger V_t shift, higher transient current, and then the lower (effective) barrier height. (ii) The larger V_{gd} exhibits higher barrier height. The larger E_{TO} corresponding to larger V_{gd} accounts for the larger gate injection, lower transient current, and then higher (effective) barrier height. (iii) N-SONOS reveals slightly higher barrier height. The larger gate injection from N^+ gate accounts for the larger Φ_t for ERS. The higher Φ_1 suggests the smaller electron injection from P-substrate than that from N-well for PGM.

IV. CONCLUSIONS

Transient current models have been extracted with time and field dependence and proven for P- and N-SONOS. The time dependence follows asymptotic t^{-1} behavior with slower tunneling rate for ERS than PGM. The field dependence follows FNT in higher field for PGM and intermediate field for ERS with relatively higher corner field for saturation. The physics-based models are useful for SONOS cell device design for PGM and ERS speed optimization.

References

[1] *Hang-Ting Lue, et al*., IEEE EDL- 25, p.816, 2004.
[2] *Anirban Roy*, *et al*., IEEE EDL-37 p.1054, 1990.
[3] *Jyh-Kuang Lin, et al*., JJAP, 32, p.2748, 1993.
[4] *H. Bachhofer, et al*., JAP, 89, p.2791, 2001.

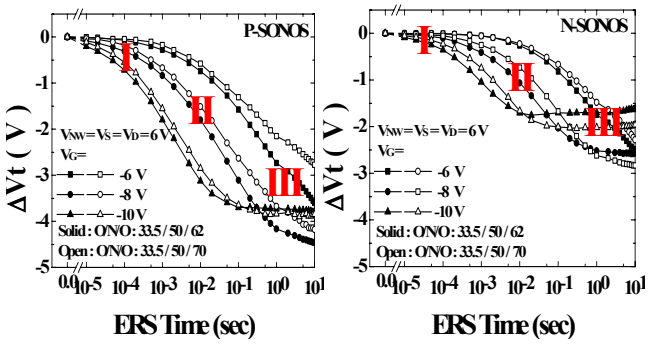

Fig.1. ERS characteristics of P-SONOS and N-SONOS devices. Thicker top oxide results in slower ERS speed.

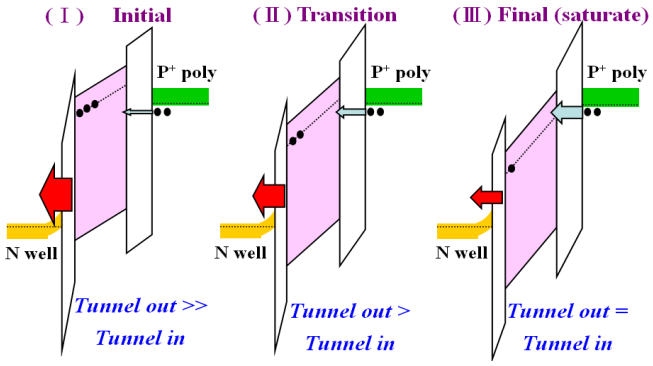

Fig.2. Band diagrams of P-SONOS device during ERS process.

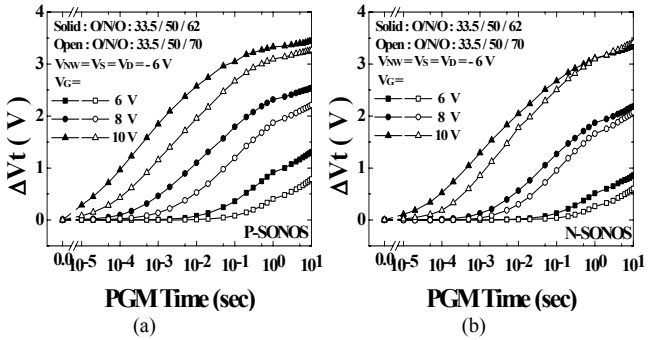

Fig.3. PGM characteristics of (a) P-SONOS and (b) N-SONOS devices. Thicker top oxide results in slower PGM speed.

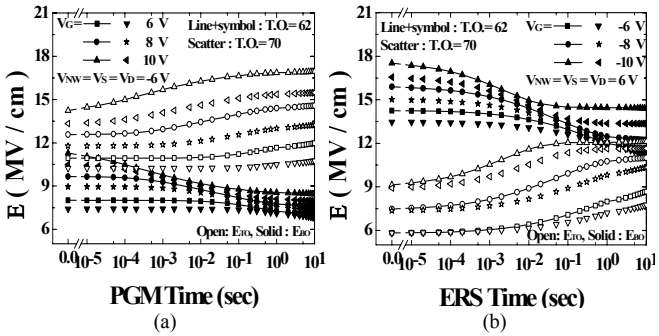

Fig. 4. Calculated electric fields of P-SONOS during (a) PGM and (b) ERS.

Items \ Device Type	P-SONOS		N-SONOS	
Bottom Oxide (Å)	33.5		33.5	
Nitride (Å)	50		50	
Top Oxide (Å)	62	70	62	70

Table 1. ONO thickness of the measured devices.

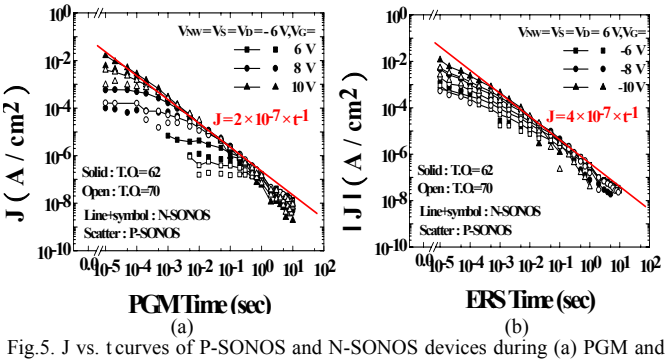

Fig.5. J vs. t curves of P-SONOS and N-SONOS devices during (a) PGM and (b) ERS. The current density at extended long PGM time follows the inverse t model given by $J = 2\times10^{-7}$ As/cm^2 x t^{-1} and at medium ERS time follows $J = 4\times10^{-7}$ As/cm^2 x t^{-1}.

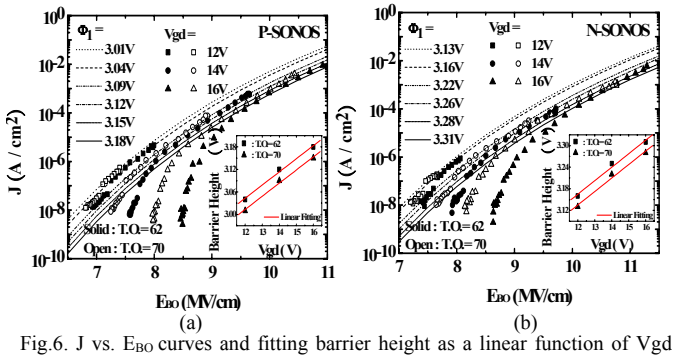

Fig.6. J vs. E_{BO} curves and fitting barrier height as a linear function of Vgd (insertion) of (a) P-SONOS and (b) N-SONOS devices during PGM.

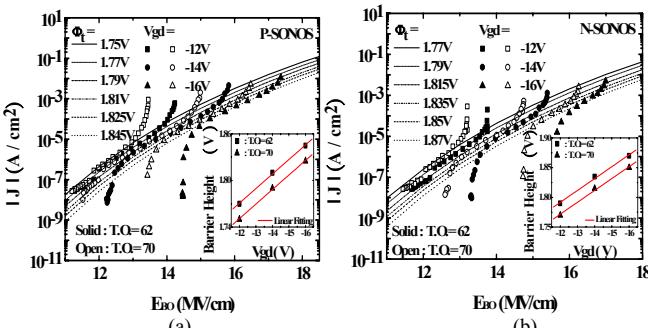

Fig.7. J vs. E_{BO} curves and fitting barrier height as a linear function of Vgd (insertion) of (a) P-SONOS and (b) N-SONOS devices during ERS.

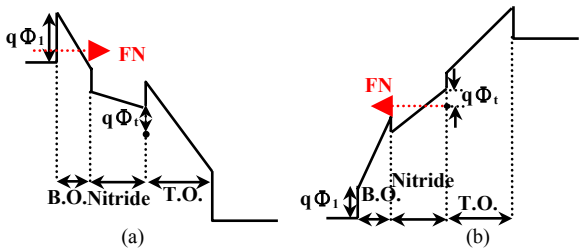

Fig.8. Tunneling band diagrams and fitting barrier eight parameters under (a) PGM and (b) ERS.

Operation \ Device Type	P-SONOS	N-SONOS
PGM (Program) Electron injection from substrate to SiN	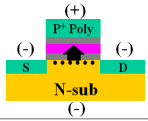	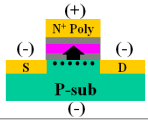
ERS (Erase) Electron ejection from SiN to substrate	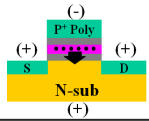	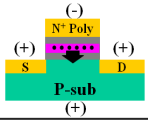

Table 2. F-N operation schemes of P-SONOS and N-SONOS devices.